ChemComm
Chemical Communications

Accepted Manuscript

This article can be cited before page numbers have been issued, to do this please use: M. Gong, J. Yang, Y. Li and J. Gu, *Chem. Commun.*, 2020, DOI: 10.1039/D0CC02872J.

ROYAL SOCIETY OF CHEMISTRY

rsc.li/chemcomm

View Article Online
DOI: 10.1039/D0CC02872J

COMMUNICATION

Glutathione-responsive nanoscale MOFs for effective intracellular delivery of anticancer drug of 6-mercaptopurine

Received 00th January 20xx,
Accepted 00th January 20xx

DOI: 10.1039/x0xx00000x

Ming Gong,[a] Jian Yang,[a] Yongsheng Li[a] and Jinlou Gu*[a]

A glutathione-triggered drug delivery system (DDS) based on nanoscale metal-organic framework (NMOF) is developed, which features an intracellular redox-responsive release of anticancer drug. Compared to normal cells, current NMOF-based DDS performs a 3-fold higher cytotoxicity to cancer cells, prefiguring its great potentials for selective cancer therapy.

Since cancer has become a serious worldwide threat to human health, various drug delivery systems (DDSs) towards cancer treatment have been explored.[1] Although the chemotherapy based on traditional DDSs is serving as a principal method in clinical therapy, its undesirable side effects remain a major problem due to the premature drug release.[2] To overcome this limitation and improve the therapeutic efficacy, advanced DDSs with stimulus-response are gradually designed, which could release the encapsulated drugs upon certain exogenous (*i.e.,* light and temperature) or endogenous (*i.e.,* pH and glutathione (GSH)) triggers.[3] To date, several carriers such as metals and quantum dots have joined into the class of advanced DDSs to meet the requirements of specific drug delivery.[4] However, the drawbacks of low loading capabilities significantly prevent their further application. Therefore, a stimulus-responsive nanoplatform with high cargo capacity is highly desirable for more efficient cancer therapy.

Thanks to the large pore volume, easy functionalization and excellent biocompatibility, nanoscale metal-organic frameworks (NMOFs) have attracted great interest in biological fields.[5] NMOFs-based advanced DDSs are emerging as the superior candidates since they could achieve spatially and temporally controllable drug release. Considering the intrinsically reductive microenvironment inside solid tumors, in which the GSH concentration (0.5-10 mM) is significantly higher than extracellular matrices and normal cells,[6] the premature drug release in normal tissues could be effectively avoided using GSH-responsive NMOFs. We suppose this suite of characteristics would render the reducible NMOFs valuable for tumor-specific drug delivery.

In this work, a thiol-functionalized NMOF, UiO-66-$(SH)_2$ is employed as a new type of redox-sensitive DDS, which is composed of zirconium ion (Zr^{4+}, metal node), 2,5-disulfanylterephthalic acid (BDC-$(SH)_2$, organic ligand) and benzoic acid (BA, modulator). During the MOFs synthesis, BA would compete with BDC-$(SH)_2$ to coordinate on Zr_6 clusters, which effectively controls the crystal growth of NMOFs and leads to the formation of small particle size. Meanwhile, the internal pore volume could be increased after the removal of the BA modulator. In this case, a thiol-containing anticancer drug, 6-mercaptopurine (6-MP), could be stably loaded into the NMOF via the formation of disulfide bonds between the thiol groups on BDC-$(SH)_2$ and 6-MP (**Scheme 1**). This smart NMOF-based DDS has several advantages: (1) the small particle size could be elaborated through the modulation of the BA contents, which provides the rapid and effective internalization for tumor cells. (2) The hierarchical pores inside the NMOF could be produced after the removal of BA, offering sufficient space for the diffusion of drug and GSH. (3) The disulfide bonds inside the NMOFs could only be cleaved in the presence of GSH, resulting in a GSH-responsive release of 6-MP. As expected, the drug-loaded NMOF showed an interesting intracellular redox-responsive drug release capability. A 3-fold higher cytotoxicity towards cancer cells

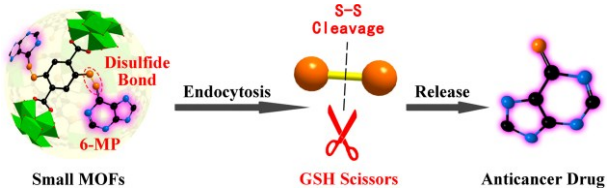

Scheme 1 The schematic diagram for the GSH-responsive drug release from small MOF particles. The high concentration of GSH in tumor cells acts as the scissors and reduces the disulfide (S-S) bonds, thus triggering the release of anticancer drug 6-MP.

[a] *Shanghai Engineering Research Center of Hierarchical Nanomaterials, Key Laboratory for Ultrafine Materials of Ministry of Education, School of Materials Science and Engineering, East China University of Science and Technology, Shanghai 200237, China. E-mail: jinlougu@ecust.edu.cn.*

Electronic Supplementary Information (ESI) available: Experimental details, ^{1}H NMR, XRD, SEM, DLS, UV-vis, fluorescence spectra and flow cytometric. See DOI: 10.1039/x0xx00000x

than normal ones were revealed from the IC_{50} (half-maximal inhibitory concentration) values, which displays the excellent tumor-selective chemotherapy. Such smart DDS would provide great convenience of MOFs for more biological applications.

To endow the MOF with redox-responsive property, the thiol-containing organic ligand BDC-$(SH)_2$ was prepared from 2,5-dihydroxyterephthalic acid diethyl ester (**Fig. S1**) and confirmed by ^{1}H NMR measurement (**Table S1**).[7] Then, UiO-66-$(SH)_2$ was synthesized solvothermally. Powder XRD technique was utilized to track the structural evolvements under different amounts of the modulator (**Fig. 1A**). All the as-synthesized MOFs exhibit similar Bragg diffraction peaks present at 2ϑ = 7.3 and 8.4° in comparison to the simulated UiO-66 structure, which correspond to the octahedral and tetrahedral cages in the frameworks of UiO-66.[8] As the feed ratio of BA/BDC-$(SH)_2$ increases from 40 : 1 to 70 : 1, the peak intensity at 2ϑ = 7.3° shows a 17-fold enhancement as shown in the amplified XRD spectra, which indicates the increased crystallinity of the synthesized MOFs. Furthermore, since the full-width at half maximum (FWHM) is inversely proportional to the crystallite size according to the Scherrer equation,[9] the gradual growth of the particle diameter could be inferred from the reduced FWHM listed in **Table S2**. Among all, the uniform MOF particles with the small size of 40 nm are visible from the SEM images (**Fig. 1B**) when the feed ratio of BA/BDC-$(SH)_2$ reaches 50 : 1. Such monodispersed nanoparticles are fully instrumental in rapid cellular endocytosis. However, both inadequate and excess dosages of BA would yield negative impacts on the morphology evolvement such as severe aggregation and inhomogeneous diameter. Therefore, the optimal feed ratio of BA/BDC-$(SH)_2$ is chosen as 50 : 1 to balance the good crystallinity and small size.

The drug loading process was conducted by a mercaptopurine oxidation and a disulfide bond exchange.[10] 6-MP was firstly oxidized to a dimer form as MP-SS-MP (1,2-di(purin-6-yl)disufane), which would further react with the thiol groups on the ligand of UiO-66-$(SH)_2$. Thus, the adequate porosity of the NMOF is of great importance. The typical type I isotherm shows the presence of massive micropores in the UiO-66-$(SH)_2$ framework (**Fig. 2A**).[11] However, this narrow pore width (< 1 nm) strongly prohibits the inner loading of the drug molecules. Therefore, a HCl-activating procedure is introduced to remove the BA modulator coordinated on the Zr clusters, further increasing the volume of the pore channels.[12] Obviously, two hierarchical pores of 1.5 and 2.7 nm (**Fig. 2B**) are created, which are larger than the dimension of the MP-SS-MP dimer (1.29 nm × 0.17 nm × 0.89 nm).[13] As a result, the drug molecule 6-MP could be effectively linked to the ligands of NMOF. The surface area significantly decreases from 517 to 250 m^2 g^{-1}, indicating the partial occupation of 6-MP to the pore space. The retained high pore volume of 0.70 cm^3 g^{-1} ensures the accessibility of 6-MP to the intracellular GSH, which is beneficial to its redox-responsive drug release.

The successful loading of 6-MP was validated by FT-IR measurement (**Fig. 2C**). The presence of thiol groups on 6-MP and UiO-66-$(SH)_2$ were affirmed by the weak characteristic peaks at the wavenumber of 2570 cm^{-1}.[14] After the reaction of 6-MP with NMOF, this peak completely disappears. At the same time, a new characteristic peak appears in the spectrum of UiO-66-SS-MP at the wavenumber of 1336 cm^{-1}, corresponding to the C-N stretching vibration on 6-MP.[15] These results indicate that the drug has been successfully grafted in the frameworks of UiO-66-$(SH)_2$ through the formation of a disulfide bond between the thiol groups on the drug and the ligand of NMOF. Furthermore, the zeta potential of the drug-loaded NMOF increases from -47.2 to -30.4 mV (**Fig. 2D**), which is explained by the consumption of thiol groups.[10]

To explore the interaction of 6-MP and the framework, the unfunctionalized and defective UiO-66 was synthesized (**Fig. S2**) as a control group. After the same HCl-activated process, the pore with diameter of 2.6 nm was created (**Fig. S3**) which is large enough for the drug loading. Afterwards, the drug loading efficiency of the NMOFs were measured to be 0.8 mg g^{-1} for UiO-66 and 35 mg g^{-1} for UiO-66-$(SH)_2$ based on the standard curve (**Fig. S4**).[16] Such negligible drug loading in unfunctionalized of UiO-66 demonstrates the weak adsorption

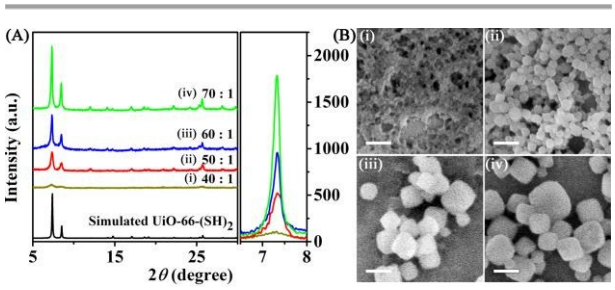

Fig. 1 (A) Powder XRD patterns (the right column shows the amplified spectra from 2ϑ = 6.5 to 8°) and (B) SEM images of UiO-66-$(SH)_2$ with different BA/BDC-$(SH)_2$ ratios: (i) 40 : 1, (ii) 50 : 1, (iii) 60 : 1 and (iv) 70 : 1. Scale bar: 100 nm.

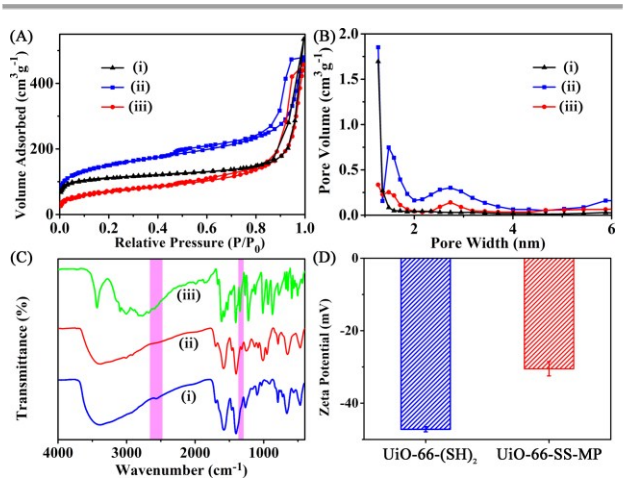

Fig. 2 (A) Nitrogen sorption isotherms and (B) the corresponding DFT pore-size distribution profiles of: (i) UiO-66-$(SH)_2$ before HCl-activated process, (ii) UiO-66-$(SH)_2$ after HCl-activated process and (iii) UiO-66-SS-MP measured at 77 K. (C) FT-IR spectra of (a) UiO-66-$(SH)_2$, (b) UiO-66-SS-MMP and (c) 6-MP. (D) Zeta potentials of UiO-66-$(SH)_2$ and UiO-66-SS-MP measured in deionized water.

capability of NMOFs towards 6-MP or its dimer MP-SS-MP. Therefore, the formation of the disulfide bond plays a key role in the drug loading process. The drug-loaded UiO-66-SS-MP remain its structural integrity, small particle size and excellent stability (**Fig. S5** and **S6**), which are the prerequisite for NMOF in biomedical applications.

Developing the redox-triggered DDS is meaningful since the GSH concentration varies significantly between the intracellular milieus of normal and cancer cells. As illustrated in **Fig. 3A**, the anticancer drug 6-MP is pre-installed in the pore of UiO-66-SS-MP via the disulfide bond. When GSH appears in the system, it would replace the encapsulated 6-MP through the formation of a new disulfide bond between the thiol groups on GSH molecule and the ligand of NMOF, simultaneously releasing 6-MP.[17] The drug release profiles could be obtained through the standard curves in different releasing environments(**Fig. S7-S9**), thanks to the separated UV-vis spectra peaks of GSH and 6-MP (**Fig. S10**). Additionally, although there is a small amount of spectra overlap between the ligand and drug (**Fig. S11**), the high stability of the NMOFs could avoid the leakage of ligand (**Fig. S12-S14**) and ensure the reliability of the drug release profiles. To measure the redox-responsiveness, the drug release profiles were tested in pH = 5.5 MES buffer solution in the presence of different concentrations of GSH (**Fig. 3B**). A rapid release could be found in the first 4 h, which is mainly attributed to the cleavage of the surface disulfide bonds. The cumulative release of 6-MP reaches 90% after 5 d of incubation with 5 mM GSH, but only 64% of 6-MP releases with 1 mM GSH. Furthermore, the release profile in the absence of GSH was also determined and a negligible release amount of 2.7% is finally found. Such a significant difference in the releasing behavior demonstrates an excellent GSH-responsive ability of UiO-66-SS-MP.

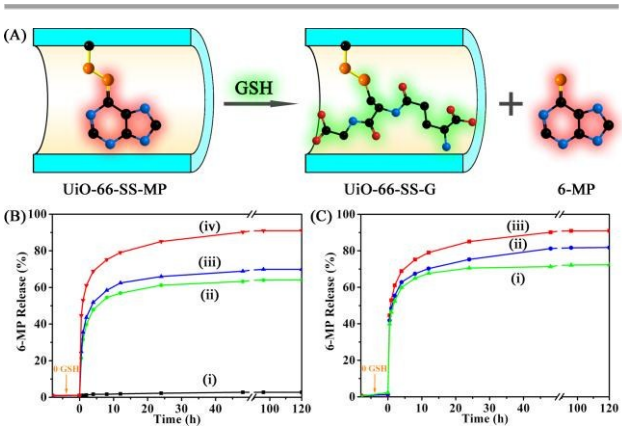

Fig. 3 (A) The release mechanism of 6-MP from UiO-66-SS-MP NMOF in the presence of GSH. The GSH molecule would replace the 6-MP and a new disulfide bond would be built between the thiol groups on GSH and the ligand of NMOF. (B) Amount of 6-MP release from UiO-66-SS-MP in pH = 5.5 MES buffer solution in the presence of different concentrations of GSH: (i) 0 mM, (ii) 1 mM, (iii) 3 mM and (iv) 5 mM. (C) Amount of 6-MP release from UiO-66-SS-MP in different pH-value buffer solutions with 5 mM GSH: (i) pH = 7.4 HEPES, (ii) pH = 6.5 MES and (iii) pH = 5.5 MES buffer solutions.

Considering the more acid milieu in cancer cells than normal cells, the 6-MP release in different pH buffer solutions was also investigated (**Fig. 3C**). Upon the addition of the same GSH concentration of 5 mM, the similar release behaviors are found in the first 4 h. However, compared to the maximum release of 6-MP at pH = 5.5 (90%), the value at pH = 7.4 is obviously lower (72%). This might be caused by the diverse reducing activity of GSH under different pH values.[18] When the pH value increases from 5.5 to 7.4, the reduced form of GSH (G-SH) trends to be converted to the deprotonated form (GS^-), which owns higher reductive activity. The released 6-MP could react to GS^- in the neutral solution easily, resulting in the GS-MP compound. On the other hand, the dimer form of GS^- itself (GSSG) would also be generated, due to the relatively higher concentration of GS^- in the solution. The large consumption of GSH in the neutral environment decreases the probability of the reaction to the encapsulated 6-MP, resulting in a reduced drug release that this work (**Fig. 3C**, **curve iii**) has shown. At the same time, the drug release from UiO-66-MP was also measured. No obvious absorbance at 324 nm assigned to the 6-MP (**Fig. S15**) further rules out the possibility of the adsorption-based drug loading in thiol-functionalized DDS.

To demonstrate the biocompatibility of UiO-66-$(SH)_2$, both NIH/3T3 normal cells and SMMC-7721 cancer cells were treated with different concentrations of NMOF. As shown in **Fig. S16**, the high cell viabilities (> 90%) verify the good biosafety of the DDS for stimulus-responsive drug delivery.

Due to the inappreciable luminescence of UiO-66-SS-MP NPs, FMN (riboflavin sodium phosphate) was selected as a fluorescent molecule which can be stably anchored onto the surface of NMOF through a strong Zr-O-P bond as our previous work shown.[19] A strong fluorescent peak at the wavelength of 537 nm could be emitted from FMN@UiO-66-SS-MP under the excitation of 405 nm. After its soaking in water for 24 h, only negligible fluorescent change could be monitored (**Fig. S17**), demonstrating the excellent optical stability of the FMN-labelled NMOFs. Then, the flow cytometry was conducted to evaluate the endocytosis behavior of FMN@UiO-66-SS-MP by SMMC-7721 cancer cells. The significant increase of the FMN fluorescence in the first 2 h (**Fig. S18**) reflects the rapid internalization of such smart DDS thanks to the small particle size. Through a further comparison of the mean fluorescent intensity (MFI) values (**Fig. S19**), a time-dependent uptake property could be revealed from the much higher fluorescent intensity (*ca.* 5400) with the incubation time of 24 h than the value with the time of 2 h (*ca.* 3300).

A similar phenomenon could be also visible from laser scanning confocal microscopy (LSCM) as shown in **Fig. 4A**. The strong blue fluorescence is emitted from the DAPI-stained nucleus, and the green fluorescence is detected from the NMOF regions in cancer cells. With the prolonging of the incubation time from 2 to 24 h, the green fluorescence is noticeably enhanced (**Fig. 4A, iii** and **vii**). Such a long-time accumulation of nanocarriers offers enough opportunity for effective contact between GSH and NMOF as well as the subsequent release of 6-MP in cancer cells.

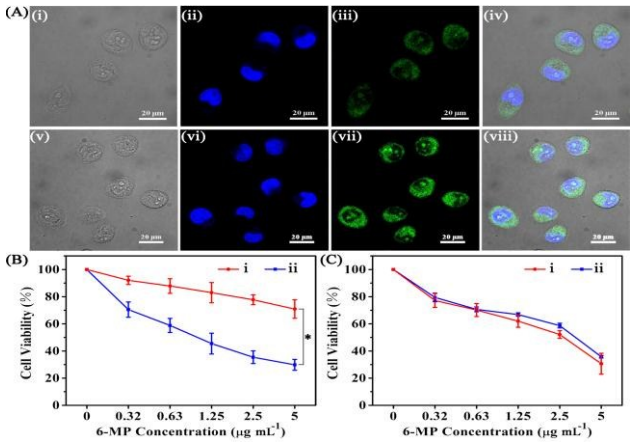

Fig. 4 (A) Confocal images of SMMC-7721 cancer cells after their incubation with 25 μg mL^{-1} NMOF for (i-iv) 2 h and (v-viii) 24 h: (i, v) the bright field, (ii, vi) the nucleus stained with DAPI, (iii, vii) NMOF labelled with FITC and (iv, viii) the merged images. Cell viabilities of (B) NIH/3T3 normal cells and (C) SMMC-7721 cancer cells incubated with (i) UiO-66-SS-MP and (ii) 6-MP at different concentrations. $^*P < 0.05$.

To testify the GSH-responsiveness, the cytotoxicity assays were conducted on both normal and cancer cells. As shown in **Fig. 4B**, more than 70% of normal cells survive in the treatment of UiO-66-SS-MP even in the high drug concentration of 5 μg mL^{-1}, in striking contrast to the low viability of 30% when stimulated with 6-MP at equivalent concentration. However, for SMMC-7721 which possess high-level expression of GSH, the cell viability of the UiO-66-SS-MP group sharply drops to 31% (**Fig. 4C**), which is similar to that of the 6-MP group (36%). The IC_{50} of UiO-66-SS-MP for SMMC-7721 is calculated to be 2.8 μg mL^{-1}, which is almost 3-fold smaller than the IC_{50} for NIH/3T3 (8.0 μg mL^{-1}). This selective cytotoxicity strongly proves the GSH-responsive release capability of UiO-66-SS-MP. It is worth mentioning that although trace amount of iodine was introduced into the NMOF, the cytotoxicity resulted from the iodine could be ignored (**Fig. S20** and **S21**).

In summary, a GSH-responsive drug-delivery platform based on NMOF was successfully developed. The resultant UiO-66-$(SH)_2$ carrier shows regular morphology and small particle diameter of 40 nm, beneficial to the rapid cellular uptake. Thanks to the redox-triggered drug release property, potent anticancer drug 6-MP can be effectively transported into the cancer cells, reducing the premature release into the blood vessel or normal cells. As a result, the cytotoxicity of such NMOF against SMMC-7721 cancer cells is almost 3-fold higher than against NIH/3T3 normal cells, realizing the purpose of selective cancer therapy. Extension of such NMOFs to introduce thiol-containing targeting molecules, might pave the way for building a broad variety of advanced targetable DDSs, and finally improve the therapy efficacy.

This work was financially supported by the Natural Science Foundation of China (21975072, 51902106, 51372084), the Natural Science Foundation of Shanghai (18ZR1408700), Projects of Shanghai Municipality (18JC1410802), the National Key Research and Development Program (2016YFC1102100) and 111 Project (B14018).

View Article Online DOI: 10.1039/D0CC02872J

Conflicts of interest

There are no conflicts to declare.

References

1 (a) X. Chen, H. Sun, J. Hu, X. Han, H. Liu and Y. Hu, *Colloids Surf. B*, 2017, **152**, 77; (b) W. Xu, G. Li, H. Long, G. Fu and L. Pu, *New J. Chem.*, 2019, **43**, 12215.

2 (a) F. Muhammad, M. Guo, W. Qi, F. Sun, A. Wang, Y. Guo and G. Zhu, *J. Am. Chem. Soc.*, 2011, **133**, 8778; (b) J. Wen, K. Yang, F. Liu, H. Li, Y. Xu and S. Sun, *Chem. Soc. Rev.*, 2017, **46**, 6024.

3 (a) P. Xing and Y. Zhao, *Small Methods*, 2018, **2**, 1700364; (b) S. Zhai, X. Hu, Y. Hu, B. Wu and D. Xing, *Biomaterials*, 2017, **121**, 41; (c) H. Chan, J. B. Ghrayche, J. Wei and A. K. Renfrew, *Eur. J. Inorg. Chem.*, 2017, **12**, 1679.

4 E. -K. Lim, T. Kim, S. Paik, S. Haam, Y. -M. Huh and K. Lee, *Chem. Rev.*, 2015, **115**, 327.

5 (a) Z. Yang, T. -A. Asoh and H. Uyama, *Chem. Commun.*, 2020, **56**, 411; (b) S. Nandi, H. Aggarwal, M. Wahiduzzaman, Y. Belmabkhout, G. Maurin, M. Eddaoudi and S. Devautour-Vinot, *Chem. Commun.*, 2019, **55**, 13251; (c) B. Slater, S. -O. Wong, A. Duckworth, A. J. P. White, M. R. Hill and B. P. Ladewig, *Chem. Commun.*, 2019, **55**, 7319; (d) L. Lupica-Spagnolo, D. J. Ward, J. -J. Marie, S. Lymperopoulou and D. Bradshaw, *Chem. Commun.*, 2018, **54**, 8506; (e) I. A. Lázaro, S. A. Lázaro and R. S. Forgan, *Chem. Commun.*, 2018, **54**, 2792; (f) I. A. Lázaro and R. S. Forgan, *Coord. Chem. Rev.*, 2019, **380**, 230.

6 J. Zhao, Y. Yang, X. Han, C. Liang, J. Liu, X. Song, Z. Ge and Z. Liu, *ACS Appl. Mater. Interfaces*, 2017, **9**, 23555.

7 L. Vial, R. F. Ludlow, J. Leclaire, R. Pérez-Fernández and S. Otto, *J. Am. Chem. Soc.*, 2006, **128**, 10253.

8 (a) I. Ahmed, K. K. Adhikary, Y. -R. Lee, K. H. Row, K. -K. Kang and W. -S. Ahna, *Chem. Eng. J.*, 2019, **370**, 792; (b) V. V. Butova, A. P. Budnyk, K. M. Charykov, K. S. Vetlitsyna-Novikova, C. Lamberti and A. V. Soldatov, *Chem. Commun.*, 2019, **55**, 901.

9 J. Ren, X. Dyosiba, N. M. Musyoka, H. W. Langmi, M. Mathe and S. Liao, *Coord. Chem. Rev.*, 2017, **352**, 187.

10 X. Jia, J. He, L. Shen, J. Chen, Z. Wei, X. Qin, D. Niu, Y. Li and J. Shi, *Nano Lett.*, 2019, **19**, 8690.

11 S. Dissegna, R. Hardian, K. Epp, G. Kieslich, M. -V. Coulet, P. Llewellyn and R. A. Fischer, *CrystEngComm*, 2017, **19**, 4137.

12 P. Deria, W. Bury, J. T. Hupp and O. K. Farha, *Chem. Commun.*, 2014, **50**, 1965.

13 Q. Zhao, C. Wang, Y. Liu, J. Wang, Y. Gao, X. Zhang, T. Jiang and S. Wang, *Int. J. Pharm.*, 2014, **477**, 613.

14 L. Xiong, D. Lan, H. Liang, L. Chen and Q. Wang, *Mater. Lett.*, 2018, **211**, 296.

15 H. Kaur, G. C. Mohanta, V. Gupta, D. Kukkar and S. Tyagi, *J. Drug Delivery Sci. Technol.*, 2017, **41**, 106.

16 X. Zhang, F. Dua, J. Huang, W. Lu, S. Liu and J. Yu, *Colloids Surf. B* 2012, **100**, 155.

17 W. Cai, J. Wang, C. Chu, W. Chen, C. Wu and G. Liu, *Adv. Sci.*, 2019, **6**, 1801526.

18 H. Zheng, Y. Rao, Y. Yin, X. Xiong, P. Xu and B. Lu, *Carbohydr. Polym.*, 2011, **83**, 1952.

19 J. Yang, X. Chen, Y. Li, Q. Zhuang, P. Liu and J. Gu, *Chem. Mater.*, 2017, **29**, 4580.

View Article Online
DOI: 10.1039/D0CC02872J

Glutathione-responsive nanoscale MOFs for effective intracellular delivery of anticancer drug of 6-mercaptopurine

Ming Gong [a], Jian Yang [a], Yongsheng Li [a] and Jinlou Gu*[a]

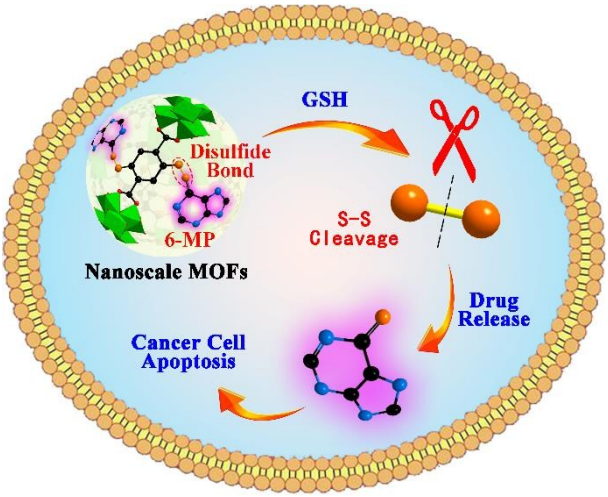

A glutathione-responsive drug-delivery platform based on nanoMOF was developed for the selective cancer therapy through the introduction of disulfide bonds.